ON THE GRAVITATIONAL FIELDS OF PANDORA AND PROMETHEUS

KRZYSZTOF GOŹDZIEWSKI and ANDRZEJ J. MACIEJEWSKI
Institute of Astronomy, Nicolaus Copernicus University, Toruń, Poland

(Received 17 October 1994)

Abstract. Utilizing topographic models of Saturn's F-ring shepherd satellites Prometheus (S16 1980S27) and Pandora (S15 1980S26), derived by Stooke (1994), and supposing that their mass density is constant, we derived basic geometrical and dynamical characteristics of the moons. They include the volume and mass, the mean radii, the tensor of inertia, and Stokes coefficients of the harmonic expansions of external gravitational potential. The best fitting ellipsoid approximations of the topography were calculated. A simple method of determining the gravitational potential on the surface of an irregular satellite is presented. Examples of equipotential surfaces of the satellites are shown

Key words: Prometheus, Pandora, Gravitational Field, Topography

1. Introduction

In this work we investigate dynamical and gravitational properties of Saturn's F-ring shepherd satellites Prometheus (S16 1980S27) and Pandora (S15 1980S26). Because of their influence on the ring structure, the moons are of primary interest and are intensively investigated (Yoder *et al.*, 1981).

Recently, Stooke (1994), using photographic images made by Voyager spacecrafts, modeled detailed shapes of the satellites. The topographic data are represented as sets of spherical cartographic coordinates of points lying on surfaces of the moons. The values of topographical radii are given for equally spaced intervals ($5^\circ \times 5^\circ$) of latitude and longitude.

The axes of the ellipsoid which approximates the shape of Pandora (see Figures 1, 2) are determined by Stooke (1994) to be $114 \times 84 \times 62$ km. Prometheus is a much more irregular body (see Figures 3, 4), with overall dimensions $145 \times 85 \times 60$ km. It is an unusually elongated body – its longest-to-shortest axis ratio is greater than 2.

The mean density of the moons estimated by Stooke (1994) and Yoder *et al.* (1981) is 0.7 ± 0.1 g/cm^3. We assume that density distribution of the two bodies is constant and uniform. This assumption was made because of the lack of reasonable models of the distribution.

The plan of this paper is as follows. In Sections 2, 4, 5 we describe results derived by application of the same methodology as in our previous paper on gravitational field of Jovian satellite Amalthea (Goździewski *et al.*, 1994). Under assumption of a constant and uniform density of a moon, explicit relationships between basic geometrical and dynamical characteristics, and the harmonic expansion of topog-

Earth, Moon and Planets **69:** 25–50, 1995.

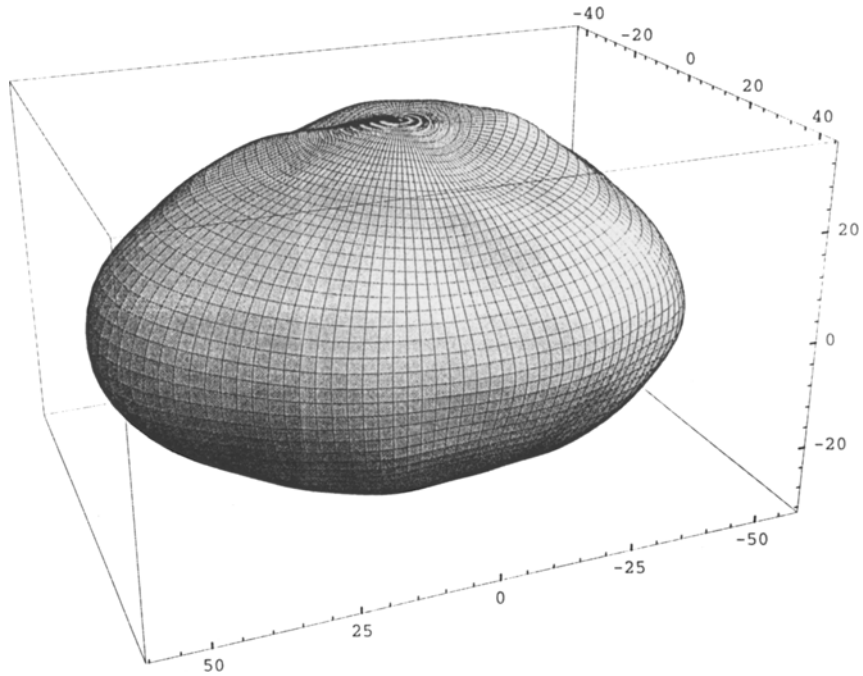

Fig. 1. The shape of Pandora defined by harmonic expansion of topography of the degree and order 18. Scale in kilometers, sub-Saturn point on the left.

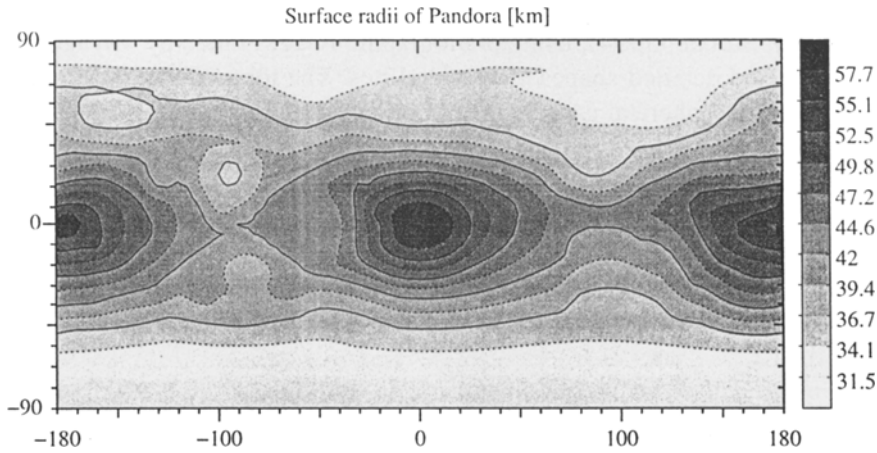

Fig. 2. Radii to the surface of Pandora, defined by the model of Stooke.

raphy may be derived (short overview of the theoretical background is given in Appendices A, B, C and D, for details see the paper cited).

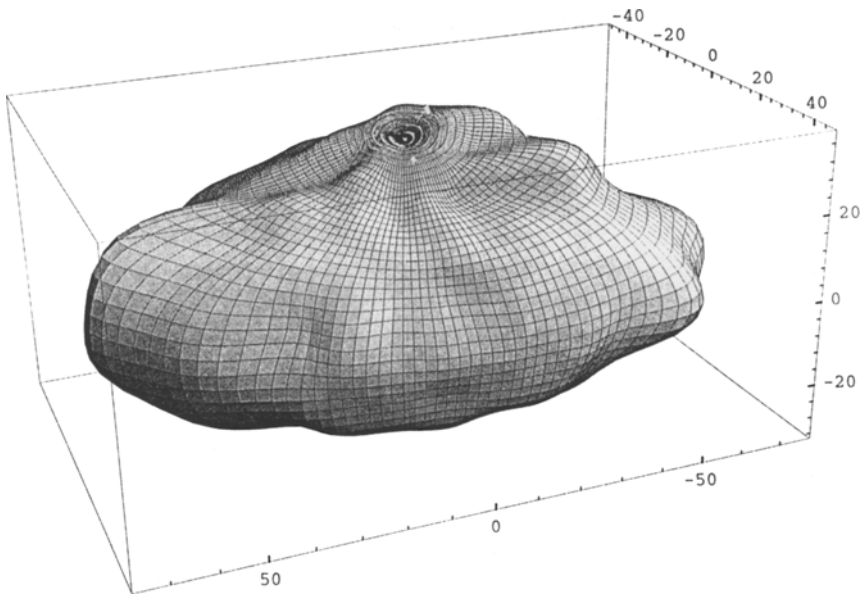

Fig. 3. The shape of Prometheus defined by harmonic expansion of topography of the degree and order 25. Scale in kilometers, sub-Saturn point on the left.

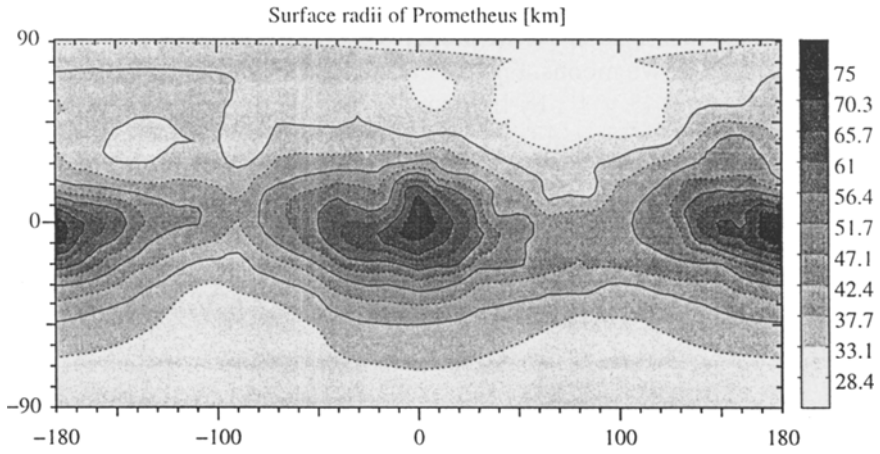

Fig. 4. Radii to the surface of Prometheus, defined by the model of Stooke.

In Section 3 we propose a simple and efficient algorithm designed for computation of parameters of an ellipsoid which best fits the topography of an irregular body. It is an alternative to the method described by Martinec *et al.* (1989).

Stokes expansion could not be applied for a representation of gravitational potential on the surface of a moon. For this purpose, we worked out an efficient,

reliable and simple algorithm of computing the potential by numerical integration. It is described in Section 6. We show also some tests of the method.

Section 7 is devoted to definition and evaluation of equipotential surfaces of the moons. In the context of our results, we discuss applicability of dynamic heights scale, introduced by Thomas (1994), for the case of Prometheus. Maps of selected equipotential surfaces of the moons are presented.

2. Harmonic Expansion of Topography

The models of the moons' shapes obtained by Stooke were first transformed to the right-handed planetocentric reference frame, and we will treat the sets of transformed data as the original ones.

Sets of harmonic models of topography (see Formula (A.1)) with varying maximal order $j_{\max}$ were derived by linear least squares fit on the basis of the discrete description of the shapes. For shorter notation we shall call the harmonic expansion of topography by HET. Natural limit of the maximal possible order of HET is determined in our specific case by the grid $5^\circ \times 5^\circ$ of angular coordinates. It is equal to 35. For $j_{\max} \geq 36$ the matrix of normal equations becomes singular.*

Errors of spectral harmonic coefficients were computed in a purely formal way, i.e., for a given moon we assumed uniform value of STD error of radii, equal 10 km for all of its control points.

Figures 5 and 6 demonstrate some properties of the harmonic models of topography derived for the two moons. Figures 5a and 6a show mean deviations of radii calculated on the grid $1^\circ \times 1^\circ$, by linear interpolation on the basis of the control points, from the radii computed from HET, as the function of maximal degree of the expansion. Apparently, we achieve very good accuracy. However, these two figures hide the fact that HET may deform the topography of an object in some regions of its surface. This is illustrated in Figures 5b and 6b where we show the

* This may need a short explanation. The harmonic model of topography is linear with respect to the unknown parameters, i.e., it has the form:

$$y(\mathbf{x}) = \sum_{k=1}^{M} a_k X_k(\mathbf{x}),$$

where M denotes a number of spectral coefficients a_k, X_k are the basis functions, $\mathbf{x}$ denotes coordinates of a control point. The design matrix of the fitting problem is:

$$A_{ij} = \frac{X_j(\mathbf{x}_i)}{\sigma_i}.$$

In a special case one of X_k, $k = 1, \ldots, M$ involves a factor $\sin(j\lambda_i)$ (see formula A.1). Because spacing of the original data is $\Delta\lambda = 5^\circ$, we have that $\lambda_i = i\Delta\lambda$, $i = 0, \ldots, 72$. For $j = 36$ argument of the trigonometric factors in the basis functions becomes $j * \lambda_i = i * 180^\circ$. Thus for $j_{\max} \geq 36$ one column of the design matrix A contains zeros.

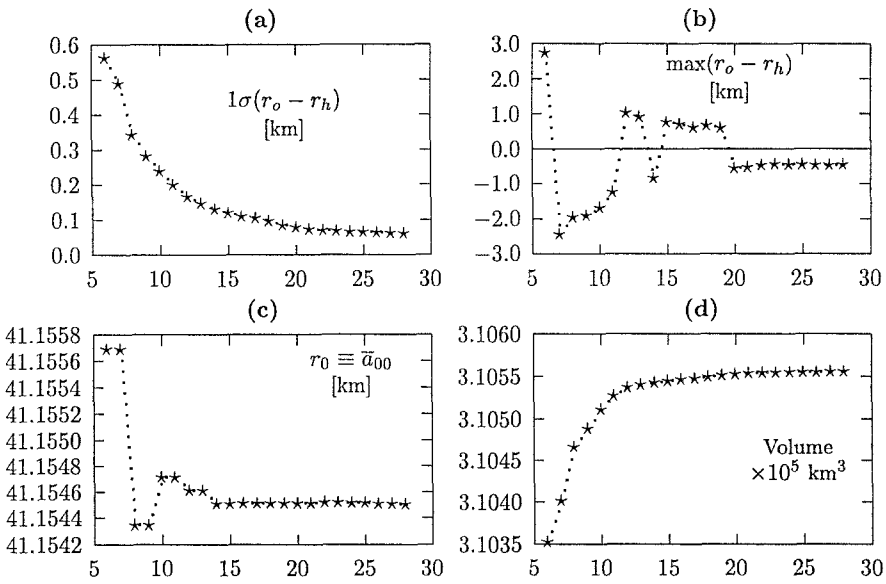

Fig. 5. PANDORA. (a) Mean errors of harmonic expansion of topography (HET). (b) Maximal deviations between HET 18 × 18 and linear interpolation of original data (evaluated at the grid 1° × 1°). (c,d) Convergence of the mean radius and volume with maximal degree of HET.

maximal deviations between the radii, linearly interpolated on the grid of control points (r_0), and computed from the harmonic expansion (r_h). They are also evaluated at the grid 1° × 1°. The deviations are 10 times greater in magnitude than the mean errors. It can be also seen that the maximal differences have almost stable values for $j_{\max} > 22$ (Prometheus), and $j_{\max} > 18$ (Pandora). Another test of the models is presented in Figures 5c, d and 6c, d which show the dependence of the mean radii of the moons, as well as their volumes (computed from Formula (B.1)), on the maximal degree of HET.

For further calculations we selected models with $j_{\max} = 25$ for Prometheus and $j_{\max} = 18$ for Pandora. Figure 7 visualizes residuals of the models as the function of planetocentric longitude. In both cases, they are biggest in the equatorial areas close to $\lambda = 0°$ and 180°. It is evident that accurate approximation of the shapes by HET requests high degrees of the expansion.

3. Tri-axial Ellipsoid Best Fitting the Topography

In general, the ellipsoid which best fits the topography of a moon has to be described by 9 parameters: the length of semi-major axes, the vector of shift of the center-of-ellipsoid from the origin of initial reference frame, and by three angles describing the orientation of the semi-major axes. The ellipsoid could be determined if we find the minimum of the *distance* between the surface of a moon and the ellipsoid.

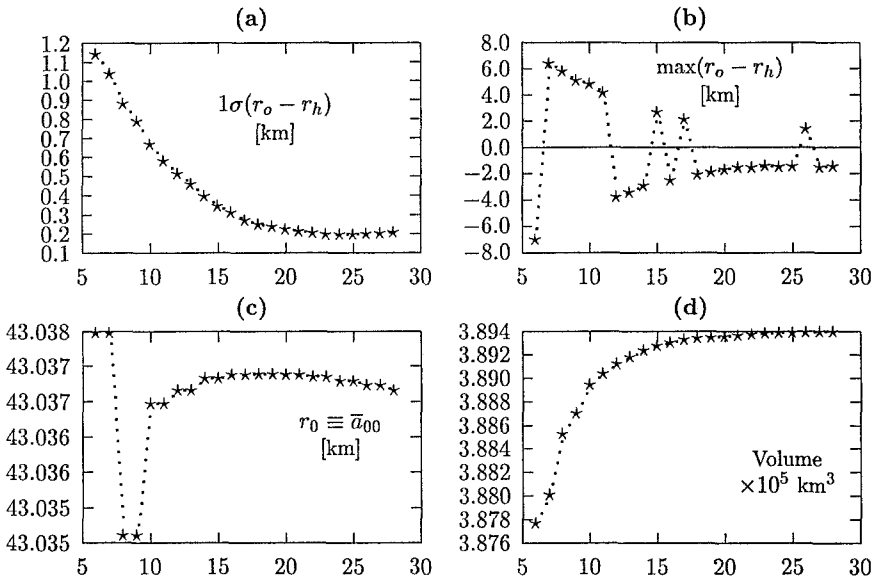

Fig. 6. PROMETHEUS. (a) Mean errors of harmonic expansion of topography (HET). (b) Maximal deviations between HET 18 × 18 and linear interpolation of original data (evaluated at the grid 1° × 1°). (c,d) Convergence of the mean radius and volume with maximal degree of HET.

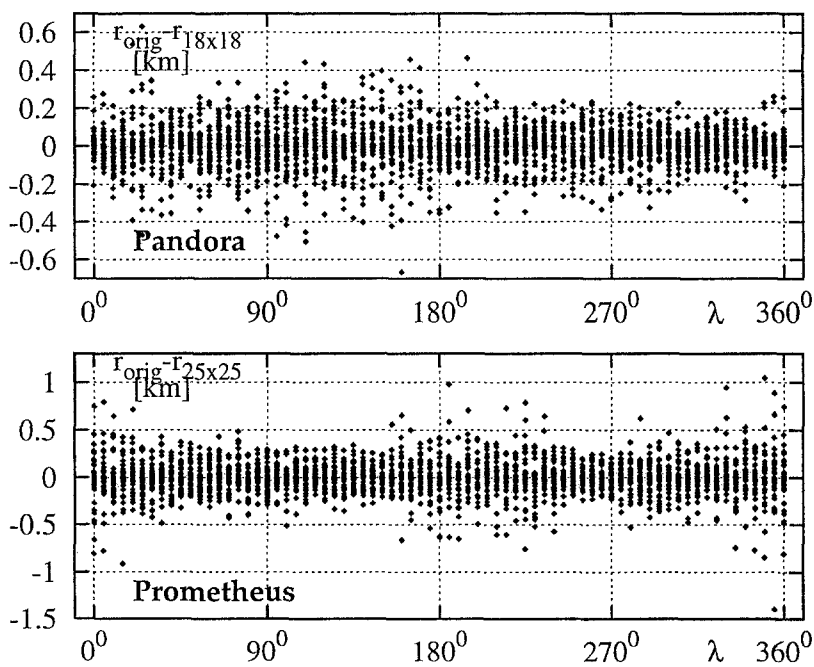

Fig. 7. Residuals of harmonic models of topography of Pandora (maximal degree 18) and Prometheus (maximal degree 25) as function of the planetocentric longitude λ. Residuals evaluated at the control points.

Formal description of such a method is complicated. An example of the fitting procedure is presented in the paper of Martineč *et al.* (1989).

In order to simplify calculations we made the following assumptions:

- we take into account only finite set, say N points of the moon surface,
- the relative shift of the center of ellipsoid is small,
- having a grid of directions to points of the moon surface we will minimize the sum of radial distances:

$$\chi^2 = \sum_{i=1}^{N} (r_t(\phi_i \lambda_i) - r_e(\phi_i, \lambda_i))^2, \tag{1}$$

where (r_t) and (r_e) are radii to the surface of the moon and the ellipsoid, respectively.

The equation of ellipsoid in its principal axes x_1, x_2, x_3 has the form:

$$\frac{x_1^2}{a^2} + \frac{x_2^2}{b^2} + \frac{x_3^2}{c^2} - 1 = 0. \tag{2}$$

By denoting $a_1 = 1/a^2$, $a_2 = 1/b^2$, $a_3 = 1/c^2$ and $\mathbf{A} = \mathrm{diag}(a_1, a_2, a_3)$, the equation of the ellipsoid can be written as $\langle \mathbf{x}, \mathbf{Ax} \rangle - 1 = 0$. The transformation from the principal axes to the reference axes is given by a real unitary matrix $\mathbf{P}$ and a translation $\mathbf{d}$:

$$\mathbf{x} = \mathbf{Py}, \qquad \mathbf{PP}^T = \mathbf{E}, \qquad \mathbf{y} = \mathbf{z} + \mathbf{d}.$$

Finally, denoting

$$\mathbf{E} = \mathbf{P}^T \mathbf{A} \mathbf{T}, \quad \mathbf{z} = r_e \begin{pmatrix} z_1/r_e \\ z_2/r_e \\ z_3/r_e \end{pmatrix} = r_e \mathbf{e} \quad \text{and} \quad \begin{aligned} \alpha &= \langle \mathbf{e}, \mathbf{Ee} \rangle, \\ \beta &= \langle \mathbf{Ee}, \mathbf{d} \rangle, \\ \gamma &= \langle \mathbf{d}, \mathbf{Ed} \rangle - 1, \end{aligned} \tag{3}$$

the equation of ellipsoid given by (2) can be written in the form

$$\alpha r_e^2 + 2\beta r_e + \gamma = 0. \tag{4}$$

Equation (4) has two roots, we choose the positive one for all directions (ϕ, λ).

As independent parameters of (1) we choose six elements of the symmetric matrix $\mathbf{E}$ and three components of the relative shift $\mathbf{d}$.

The function (1) was minimized by application of Marquardt's iterative method (Press *et al.*, 1992). As a result we obtain the matrix $\mathbf{E}$ and the shift $\mathbf{d}$. Solution of the eigenproblem for the matrix $\mathbf{E}$ gives the semi-major axes and rotation matrix $\mathbf{P}$.

Applying this procedure on input data describing the shapes of Pandora and Prometheus, we get results given in Tables II, III. In both cases the shifts of ellipsoid

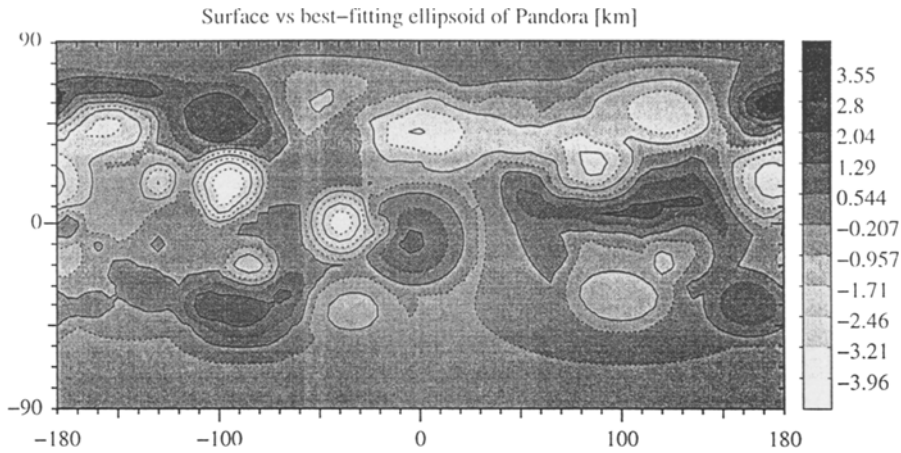

Fig. 8. Radial difference between the surface of Pandora and the best-fitting ellipsoid.

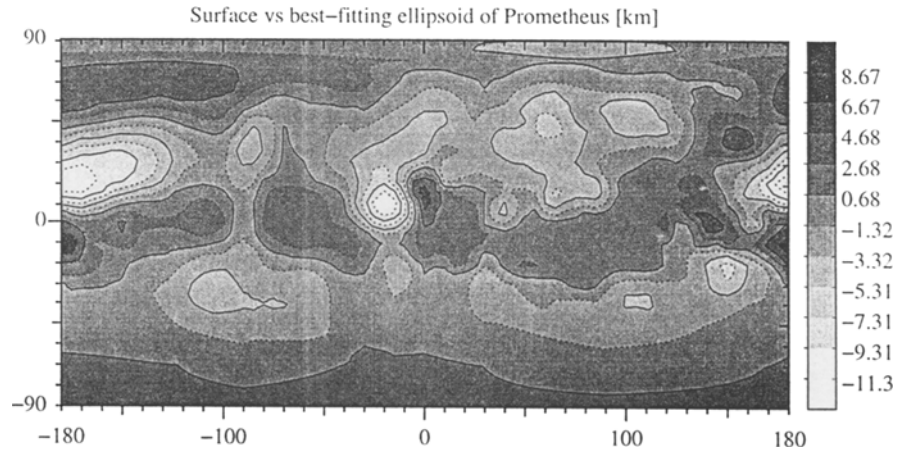

Fig. 9. Radial difference between the surface of Prometheus and the best-fitting ellipsoid.

centers with respect to the frame of the data is in the range of 1 km. Volumes of fitted ellipsoids are almost the same as volumes of the harmonic models, with accuracy better than 0.05%. Figures 8 and 9 show radial differences between the surfaces of the moons and their best-fitting ellipsoids.

4. Inertia Tensor and Principal Axes

Components of the inertia tensor per unit mass may be computed from Formula (C.1). Let us observe that their estimations converge very fast with the maximal degree of HET. Solving the eigenproblem for the inertia tensor matrix one can easily evaluate principal moments of inertia (A, B, C) and orientation of the principal

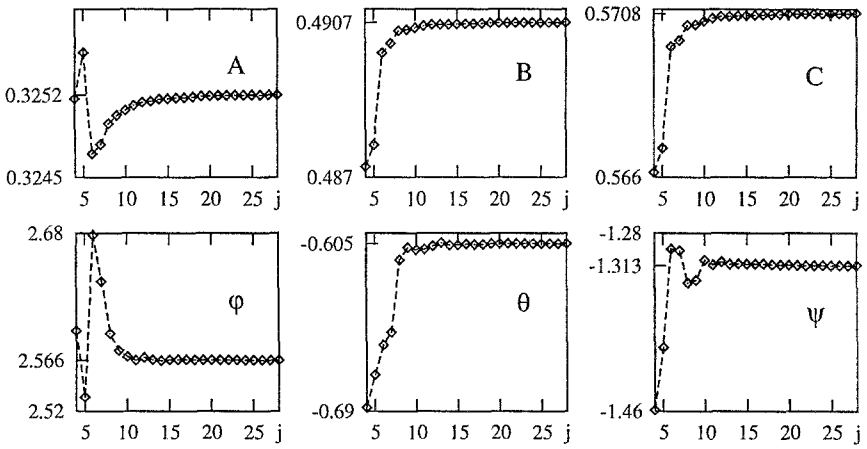

Fig. 10. Main moments of inertia (in units of Mr_0^2) for Pandora. Euler angles of the type 3-2-1 (in degrees), describing orientation of Pandora's principal axes with respect to the original reference frame.

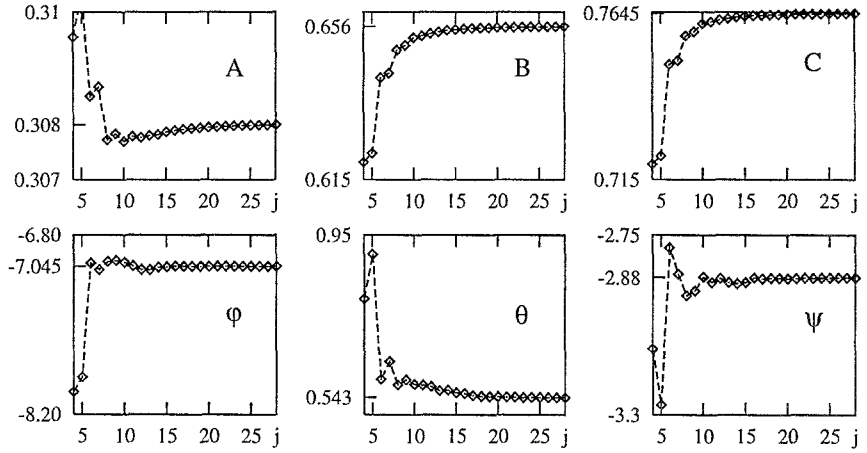

Fig. 11. Main moments of inertia (in units of Mr_0^2) for Prometheus. Euler angles of the type 3-2-1 (in degrees), describing orientation of Pandora's principal axes with respect to the original reference frame.

axes with respect to the original, planetocentric reference frame. Dependence of the quantities on the maximal degree of HET is shown in Figures 10 and 11. The principal moments of inertia are scaled by the factor Mr_0^2. For comparison we computed components (A_e, B_e, C_e) of the inertia tensor of the best fitting ellipsoids (see Tables II, III). Differences are generally small in the case of Pandora (the greatest is 1.5% for the moment B, other two less than 0.5%). Data for Prometheus show discrepancy of few percent (moments C differ by 5%).

Generalized moments of inertia of the first order and components of the inertia tensor (together with their formal uncertainties) are given in Table I.

TABLE I

Moments of inertia of the first order I_x, I_y, I_z (in units of Mr_0) and components of the inertia tensor I_{xx}, I_{yy}, I_{zz}, I_{xy}, I_{xz}, I_{yz} (in units of Mr_0^2)

	Prometheus	Pandora
I_x	0.0163 ± 0.0048	0.0086 ± 0.0048
I_y	0.0001 ± 0.0700	0.0014 ± 0.0700
I_z	0.0076 ± 0.0700	0.0016 ± 0.0700
I_{xx}	0.3132 ± 0.0079	0.3256 ± 0.0081
I_{yy}	0.6510 ± 0.0100	0.4904 ± 0.0093
I_{zz}	0.7642 ± 0.0110	0.5708 ± 0.0099
I_{xy}	0.0424 ± 0.0140	-0.0074 ± 0.0130
I_{xz}	0.0050 ± 0.0125	-0.0027 ± 0.0167
I_{yz}	0.0049 ± 0.0125	0.0017 ± 0.0167

TABLE II

Basic geometrical and dynamical characteristics of Pandora

Geometrical characteristics			
– Mean radius r_0 (km)	41.154	± 0.218	
– Maximal radius (km)	57.7	at $\lambda = 0°$,	$\phi = 0°$
– Mean equatorial radius (km)	41.248	± 0.218	
– Volume ($\times 10^5$ km^3)	3.105	± 0.062	
Inertial characteristics			
– Mean density ρ_c ($\times 10^3$ kg/m^3)	0.7 ± 0.1		
– Total mass M ($\times 10^{17}$ kg)	2.174	± 0.054	
– Shift of mass' center x, y, z (km)	0.35	0.05	0.06
– Principal moments of inertia A, B, C ($\times mr_0^2$)	0.325	0.491	0.570
– Orient. of principal axes (3-2-1 Euler angles) (deg)	2.57	-0.61	-1.31
Gravitational characteristics			
– Mean potential W_0 (m^2/s^2)	-360.0		
– Second harmonic $\overline{C}_{20}$	-7.28×10^{-2}	$\pm 9.0 \times 10^{-4}$	
Best fitting ellipsoid			
– Semi major axes (a, b, c) (km)	55.7 ± 3.4	41.3 ± 2.2	32.3 ± 1.1
– Volume ($\times 10^5$ km^3)	3.105	± 0.273	
– Main moments of inertia A_e, B_e, C_e ($\times Mr_0^2$)	0.324	0.489	0.567
– Orientation of axes (3-2-1 Euler angles) (deg)	2.67	-0.41	-2.04
– Shift of the center (km)	-0.2 ± 0.5	0.2 ± 0.4	-0.4 ± 0.2

TABLE III

Basic geometrical and dynamical characteristics of Prometheus

Geometrical characteristics			
– Mean radius r_0 (km)	43.037	± 0.218	
– Maximal radius (km)	75.0	at $\lambda = 0°$,	$\phi = 0°$
– Mean equatorial radius (km)	43.134	± 0.218	
– Volume ($\times 10^5$ km^3)	3.894	± 0.073	
Inertial characteristics			
– Mean density ρ_c ($\times 10^3$ kg/m^3)	0.7 ± 0.1		
– Total mass M ($\times 10^{17}$ kg)	2.727	± 0.065	
– Shift of mass' center x, y, z (km)	0.70	0.01	0.33
– Principal moments of inertia A, B, C ($\times$ mr_0^2)	0.308	0.656	0.766
– Orient. of principal axes (3-2-1 Euler angles) (deg)	-7.04	0.54	-2.88
Gravitational characteristics			
– Mean potential W_0 (m^2/s^2)	-419.0		
– Second harmonic $\overline{C}_{20}$	-1.261×10^{-1}	$\pm 1.4 \times 10^{-3}$	
Best fitting ellipsoid			
– Semi major axes (a, b, c) (km)	70.2 ± 4.0	42.7 ± 2.2	31.0 ± 1.0
– Volume ($\times 10^5$ km^3)	3.892	± 0.324	
– Main moments of inertia A_e, B_e, C_e ($\times M r_0^2$)	0.301	0.635	0.728
– Orientation of axes (3-2-1 Euler angles) (deg)	-7.63	0.997	-5.04
– Shift of the center (km)	-0.80 ± 0.4	0.18 ± 0.4	-0.69 ± 0.21

TABLE IV

Mean orbital elements of Prometheus and Pandora (adopted from Lang (1991))

Satellite	r_0 ($\times 10^3$ km)	r_0/R_{Planet}	Orbital Period (days)	Eccentricity (deg)	Inclination (deg)
S16 Prometheus	139.4	2.310	0.613	0.004	0.0
S15 Pandora	141.7	2.349	0.629	0.004	0.1

– Symbols description: r_0 – orbital radius, R_{Planet} – radius of the primary.
– Inclinations are relative to the planet's orbital plane.

We also determined the orientation of the principal axes reference frame, described by Euler angles of the type 3-2-1 (ϕ, θ, ψ). The principal frame of Pandora almost coincides with the geometrical frame (angles ϕ and ψ are of order

$2°$), in the case of Prometheus, the biggest angle is $\phi \approx -7°$. The orientations coincide very well with those of the best-fitting ellipsoids.

Concluding, the best fitting tri-axial ellipsoid approximation of the moons' topography seems to be quite satisfactory for dynamical studies. It very accurately preserves volumes and inertial characteristics of the moons.

5. Stokes Harmonic Coefficients

Harmonic expansions of external gravitational potential were evaluated by application of Formula (D.2) which establishes direct connection between spectral coefficients of HET and Stokes coefficients of the potential expansion.

In Figures 12 and 13 we show the dependence of some low degree Stokes coefficients of Pandora and Prometheus on the maximal degree of HET. As in the case of inertial characteristics, their convergence is very fast. It should be mention that the application of HET for evaluation of Stokes coefficients causes a rapid increase of computation time with growing maximal degree of the expansion. In this context, it is necessary to select an optimal maximal degree of the HET – it should be high enough to achieve convergence of the Stokes coefficients, but it is limited by CPU time; for example, computations of the set of Stokes harmonics up to the maximal degree 18, performed on SunSparc 10/30, took few hours of the CPU time.

For final evaluations we utilized the previously selected harmonic models of topography. On their basis, the harmonic model of gravitational potential of the degree and order 18 was constructed for Pandora. In the case of Prometheus, we derived a model with maximal degree 25. Formal STD errors of low order Stokes coefficients are in the range of few percent. However, the errors are growing fast, and for degrees >18 they are greater than 100%.

The models may be received via e-mail or on a DOS-diskette upon request, from the first author.*

6. Direct Evaluation of the Gravitational Potential

For investigations of possible connections between gravity and surface features of a moon we have to know the gravitational potential and forces on the surface. The harmonic expansion is valid for the points lying in the exterior of the small est sphere wholly covering the body. Thus, it cannot be used for the purposes mentioned.

Let us mention the works by Antonov and Kholshevnikov (1980), Petrovskaja (1979), Chujkova (1978; 1984). In these papers the authors tried to extend the

* E-mail address is chris@astri.uni.torun.pl

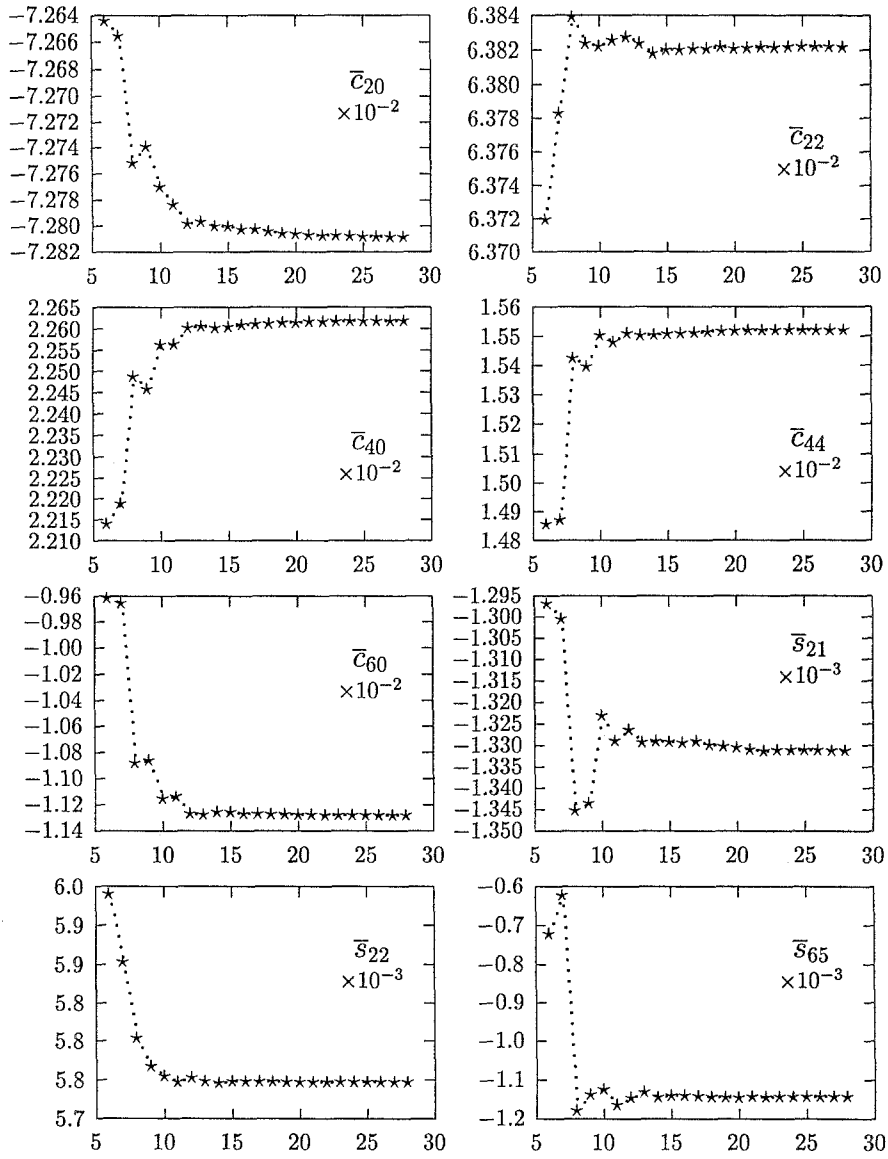

Fig. 12. Dependence of Stokes coefficients of Pandora on the maximal degree of HET.

validity of the harmonic expansion. Their conclusion, summarized shortly, is that the extension is generally possible, however, under significant restrictions:

- in order to obtain reliable results it is necessary to modify in a nontrivial way Stokes coefficients, accounting for local influence of the topography,
- the continuation is applicable in practice only in the case of Earth-like planets, i.e., those having small flattening.

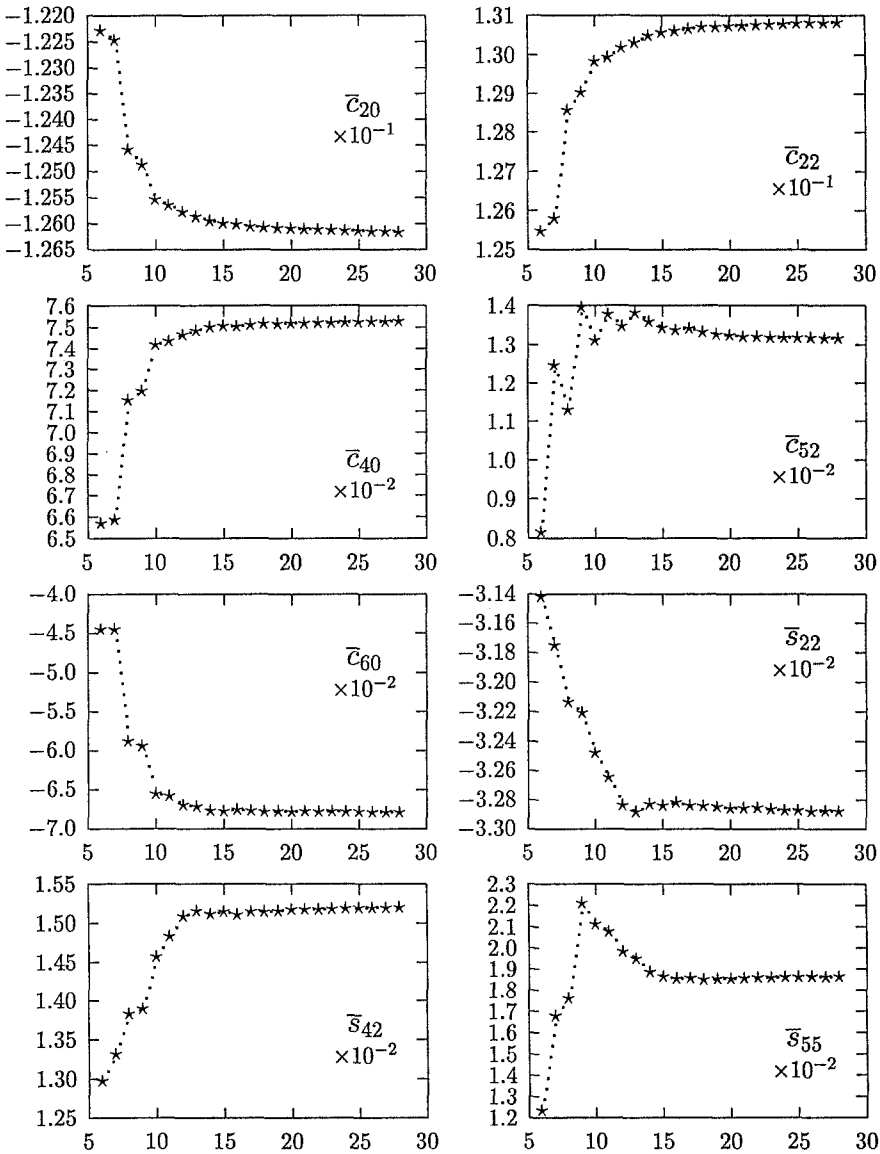

Fig. 13. Dependence of Stokes coefficients of Prometheus on the maximal degree of HET.

Recently, Werner (1994) described in details how to determine the exterior gravitational potential and acceleration components, supposing that a body having a constant density is represented as a polyhedral shape. However, in principle this method also fails on the surface of the body.

Thus, in the regions close to the surface we need another method of the gravity determination. As one of the possibilities we can choose direct numerical integration.

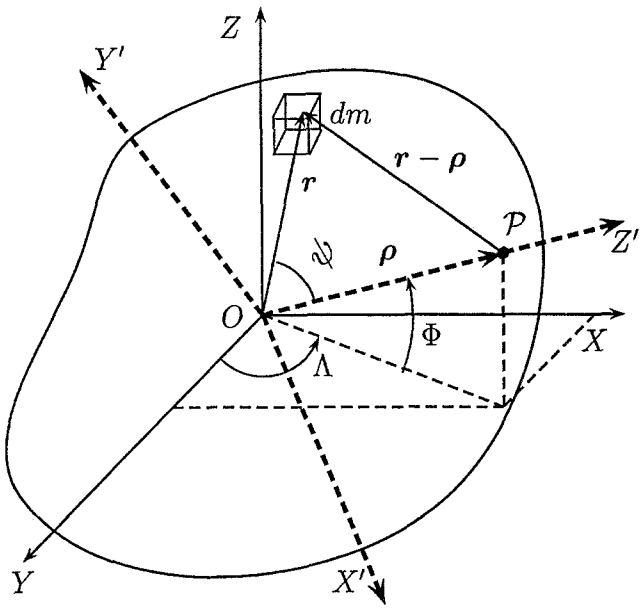

Fig. 14. Reference frames for evaluation of the gravitational potential.

Gravitational potential of a body is defined by the formula

$$V_g(\boldsymbol{\rho}) = G\sigma_c \int_\nu \frac{r^2 \cos\phi}{\sqrt{\rho^2 + r^2 - 2\rho r \cos\psi}} \, \mathrm{d}r \, \mathrm{d}\phi \, \mathrm{d}\lambda,$$

where (r, ϕ, λ) are the coordinates of the mass element, $\psi \equiv (\widehat{\boldsymbol{\rho}, \mathbf{r}})$, and let us assume that the spherical coordinates of $\boldsymbol{\rho}$ are (ρ, Φ, Λ). It is valid in every point $\mathcal{P}(\boldsymbol{\rho})$ of the space. The integral should be computed numerically, assuming that a model of shape of the body is known. This seems to be trivial, however, a practical problem arises here. If the point $\mathcal{P}(\boldsymbol{\rho})$ lies on the surface or in the interior of the body then the integrated function is singular at this point. This singularity vanishes after shifting the center of the coordinate system to the point $\mathcal{P}$ (Fitzpatrick, 1960). For practical reasons this is not satisfactory, because in the new frame it is difficult to describe the shape (thus determine the limits of integration).

To solve the problem mentioned above, we propose the following approach. Let us assume that we compute a value of the potential at the point $\mathcal{P}(\boldsymbol{\rho})$. First we rotate the reference frame in such a way that the point $\mathcal{P}$ lies on the Z-axis in the new frame (see Figure 14).

After that the angle ψ is equivalent to the latitude ϕ in the new frame. Thus, the most inner integral over variable r may be written as

$$I(\phi, \rho) = \int \frac{r^2 \cos\phi}{\sqrt{\rho^2 + r^2 - 2r\rho \sin\phi}} \, \mathrm{d}r$$

$$\equiv \rho^2 \int \frac{x^2 \cos\phi}{\sqrt{x^2 - 2x\sin\phi + 1}}\,\mathrm{d}x = \rho^2 J(\phi, x), \quad x = \frac{r}{\rho}.$$

It allows to express it in the finite form:

$$J(\phi, x) = \cos\phi \left[\left(\frac{3}{2}\sin\phi + \frac{1}{2}x \right) D(x) + \left(-\frac{1}{2} + \frac{3}{2}\sin^2\phi \right) \log(2x - 2\sin\phi + 2D(x)) \right],$$

where $D(x) = \sqrt{x^2 - 2x\sin\phi + 1}$. It is crucial that the function J has well defined limits when we approach the point $\mathcal{P}$, i.e., in the critical case:

$$\lim_{\phi \to 90^\circ} J(\phi, x) = 0.$$

Thus the computation of V_g is reduced to the evaluation of surface integral over variables (ϕ, λ). The reduction is very important because it significantly decreases the amount of computational time.

For performing computations we used Gauss–Legendre quadrature of 60th order. A simple test of the method was to integrate gravitational potential of a three-axial ellipsoid and to compare it with the result computed from an analytical formula (Danby, 1962). It showed that potential derived by numerical integration (with double precision) is precise up to $10^{-6} : 10^{-7}$ in relative scale.

6.1. Numerical integration vs harmonic expansion of the potential

Having the independent method of determining the gravitational potential we performed some tests of the harmonic model of Prometheus gravity (expansion of maximal degree and order 25).

For direct numerical integration two models of the topography were used – the HET of the degree and order 25 (model I) and the original model of Stooke, with linear interpolation (model II). The potential was evaluated on a sphere with radius 76 km. Maximal radius of Prometheus predicted by model I is 74.7 km at $\phi = 2^\circ$, $\lambda = 1^\circ$, model II sets it to 75 km at the sub-Saturn point.

Numerical integration was performed with relative accuracy 5.0×10^{-6}. It was determined by the relative difference between integrals obtained after two successive divisions of integration intervals.

Figure 15 illustrates the comparison of results derived by application of the Stokes expansion and obtained by numerical integration over the shape defined by model II. Relative differences are up to 0.5%. The same test performed on model I showed that they do not exceed 2.5×10^{-4}. In both cases, we observed the worst agreement in small equatorial areas close to the longitudes 0° and 180°. In the case

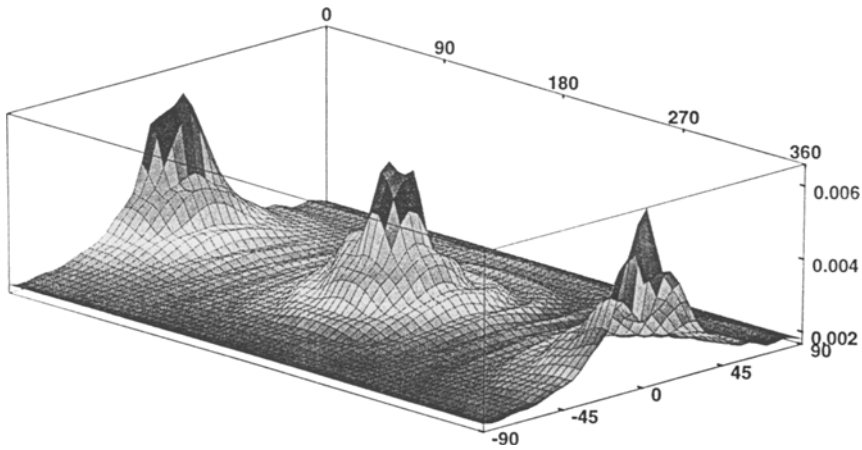

Fig. 15. Relative, absolute differences between gravitational potential of Prometheus computed by numerical integration and derived from harmonic model of the degree and order 25, on the sphere of radius 76 km.

of model II, outside these regions differences are very small – they are in the range $10^{-5} : 10^{-6}$. This may be explained by the fact that computations were performed on the basis of *the same shape*, i.e., determined by HET.

The loss of accuracy near the critical longitudes we explain twofold

- in their vicinity the test sphere passes close to the surface, thus the convergence of the Stokes expansion is slower than in more distant areas of the sphere,
- the Stokes coefficients are determined on the basis of HET, which changes significantly the shape just in the critical areas.

Another test was to evaluate by the two methods the equipotential surface passing through the sub-Saturnian point having Cartesian coordinates (95, 0, 0) km, i.e., 20 km over the surface of Prometheus. For numerical integration model II was used. In this test we took into account Prometheus gravity only.

At first, in order to make the comparison more transparent, we approximated the equipotential surface derived by numerical integration by the best-fitting ellipsoid with semi-axes 93.86, 83.14, 79.63 km, oriented with respect to the geometrical frame by 3-2-1 Euler angles $\phi = -7.2°$, $\theta = 0.7°$, $\psi = -3.3°$. Figure 16 shows radial separation of both of the equipotential surfaces from the best-fitting ellipsoid. We observe that discrepancies between the surfaces are very small.

7. Equipotential Surface

Prometheus and Pandora have very similar orbital properties. Table (6.1) describes their orbital elements. Both are in synchronous rotation with Saturn, they have negligible orbital eccentricities, and small inclination to the equator plane of the primary. This fact suggests an application of an unified model of the force field. For

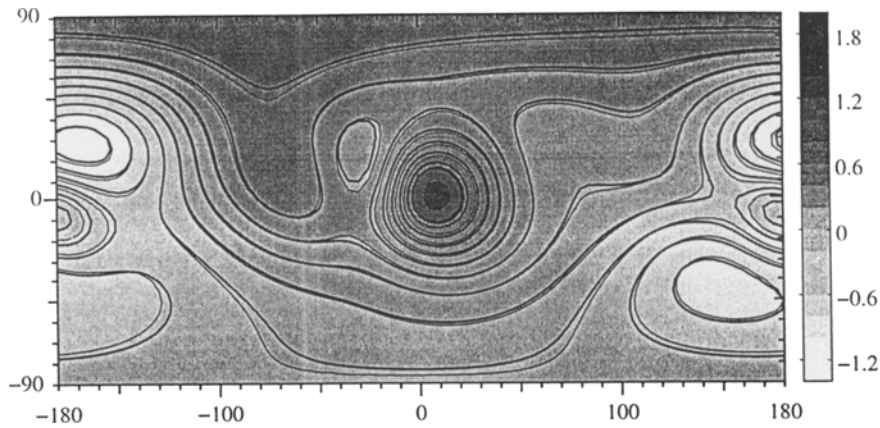

Fig. 16. Equipotential surfaces of Prometheus' gravitation relative to an ellipsoid with semi-major axes 93.86, 83.14, 79.63 km, the orientation with respect to original reference frame described by 3-2-1 Euler angles $\phi = -0.7°$, $\theta = 0.7°$, $\psi = -3.3°$. Rotation and gravity of Saturn effects were omitted. Shaded contours limited by thin lines correspond to the equipotential surface derived by numerical integration over the shape described by the model of Stooke. Thick contours represent the equipotential surface computed from harmonic expansion of the degree and order 25. Overall scale is the same for both of the surfaces, contours interval is 0.2 km.

its determination let us assume the following coordinate frame with the origin at the center of mass of a synchronously rotating satellite: X-axis is directed toward the primary (thus crossing the surface of the moon at $\phi = 0°$, $\lambda = 0°$), Z-axis has direction of rotation axis, Y-axis complements the system to the orthonormal, right-handed frame. We fix with this system spherical coordinates: radius vector $\boldsymbol{\rho}$, latitude λ measured from XY-plane, longitude ϕ measured counterclockwise from X-axis. In such a uniformly rotating frame the potential function of force field at an arbitrary point may be written as (Kutshik, 1990)

$$W(\rho, \phi, \lambda) = V_g(\rho, \phi, \lambda) + V_c(\rho, \phi, \lambda) + V_t(\rho, \phi, \lambda), \tag{5}$$

where V_g denotes pure gravitational potential of the satellite, V_c represents centrifugal potential, and V_t is tidal potential of Saturn. We are interested in static force field, so Coriolis forces are excluded. Additional effects contributing to the potential such as librations, orbit's eccentricity and inclination, nonuniform gravitational field of the primary are also neglected.

Because orbits of the satellites are almost circular, we may write (neglecting variability of rotation rate $\omega = 2\pi/T$, T – orbital period):

$$V_c(\rho, \phi) = -\frac{1}{2}\omega^2 \rho^2 \cos^2 \phi.$$

Tidal potential of Saturn may be approximated to the lowest order with respect to ρ/r_0 by the formula

$$V_t(\rho, \phi, \lambda) = -\frac{GMs\rho^2}{2r_0^3}(3\cos^2\phi\cos^2\lambda - 1),$$

where r_0 is the orbital radius, M_S denotes the mass of Saturn. Because $GM_S/r_0^3 = \omega^2$ the sum of $V_t + V_c$ is

$$V_t + V_c = -\frac{1}{2}\omega^2\rho^2[\cos^2\phi(3 + \cos^2\lambda) - 1] \text{ or } V_t + V_c = -\frac{1}{2}\omega^2(3x^2 - z^2),$$

with (x, y, z) denoting Cartesian coordinates of a point.

The equipotential surface of a moon is a set of points (ρ, ϕ, λ) defined by equation

$$W(\rho, \phi, \lambda) = W_0,$$

where W_0 is taken as an appropriate constant. As the 'geoid' of a moon we may take an equipotential surface close to its physical surface. Because the shapes of the satellites under investigation are highly irregular, we decide to take value of W_0 as the mean of the total potential evaluated at points belonging to the grid of original topographic data.

In order to determine the radius of the equipotential surface $\rho_e(\phi, \lambda)$ one has to find a root of a nonlinear equation

$$f(\rho) \equiv W(\rho, \phi, \lambda) - W_0 = 0.$$

Function $f(\rho)$ is monotonic and it has one real positive root in the vicinity of the surface. For solving the equation we used the secant method.

The results derived for Pandora and Prometheus are illustrated in Figures 17–22. Figures 17 and 20 show maps of gravitational potential V_g on the surfaces of the moons, Figures 18, 21 are maps of total surface potential W. It is evident that the tidal and rotational effects have substantial influence on the potential. They change its scale as well as its distribution over the surface. For both of the moons we may observe that distribution of the total potential is well correlated with the radial separation of the physical surface and the equipotential surface (Figures 19, 22).

According to works of Veverka (Veverka *et al.*, 1981), and recent paper of Thomas (1994), variations of gravity on the surfaces of Amalthea, Phobos and Deimos may explain the appearance of some features observed on them. For example, the variations may indicate directions of the downslope movement of regolith. For investigating such effects on the surfaces of Phobos and Deimos, Thomas (1994) used the scale of dynamic heights, defined as

$$H_d = \frac{W_1 - W_0}{g_r},$$

where W_1 and W_0 are potential energies per unit mass of the measured and reference points, g_r is a reference gravity. According to the paper cited, the dynamic

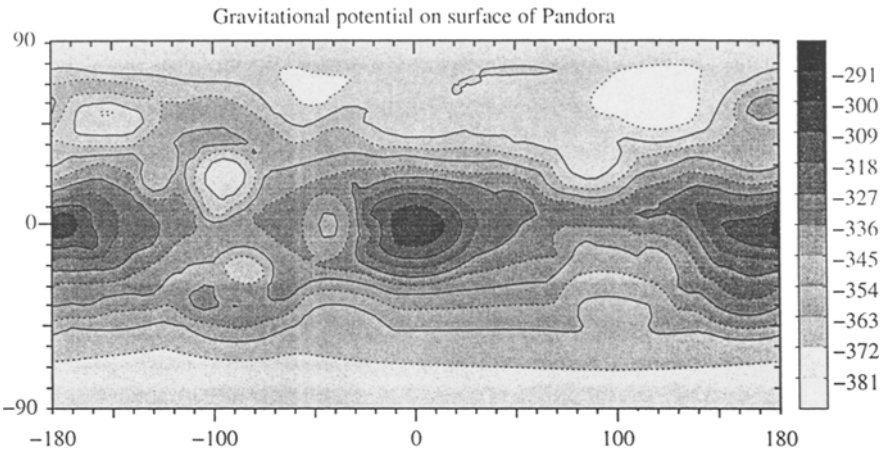

Fig. 17. The gravitational potential on the surface of Pandora (m^2/s^2).

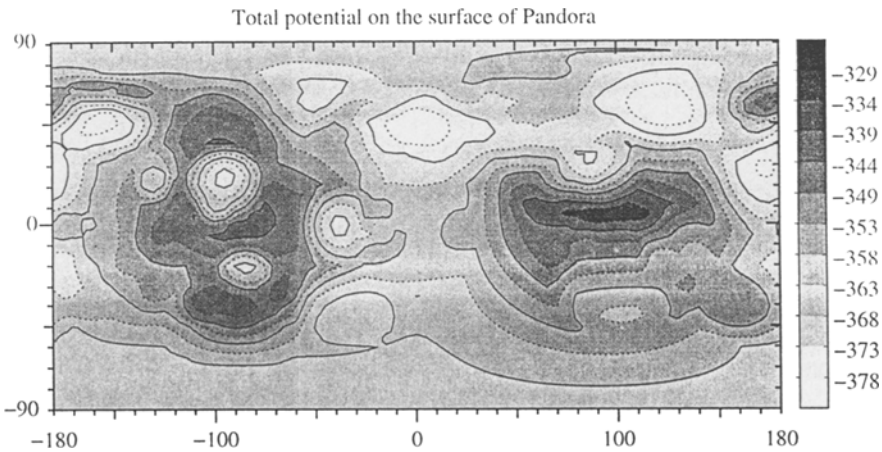

Fig. 18. The total potential (including self-gravity, rotation and tidal influence of Saturn) on the surface of Pandora (m^2/s^2).

heights better describe the downslope and upslope directions, than radial differences between the physical and equipotential surface. We did a comparison for Prometheus. Its dynamic heights were calculated under assumption of constant value of the reference gravity (following the paper of Thomas). It was determined as the mean of the gravitational acceleration on the surface, namely $g_r = 9.826 \times 10^{-3}$ m/s^2. The comparison is shown in Figure 22 and Figure 23. Apparently, structures depicted in these two figures agree very well (the different overall scale of the two characteristics is not important). Our explanation of this fact is that, as far as the dynamic heights are constructed with a constant value g_r, they do not supply qualitatively new information from this given by the radial separation of the physical and equipotential surface. A closer inspection shows that in the case when we assume

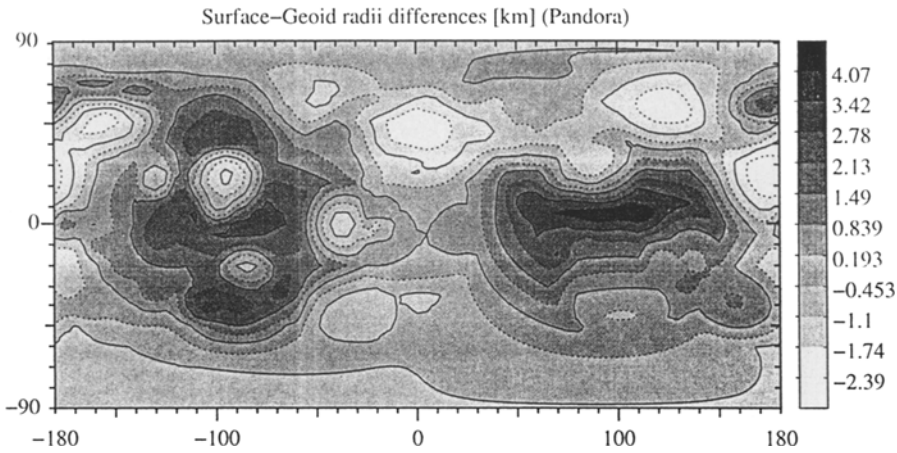

Fig. 19. Radial separation of surface of Pandora from the equipotential surface $W_0 = -360\ \mathrm{m}^2/\mathrm{s}^2$.

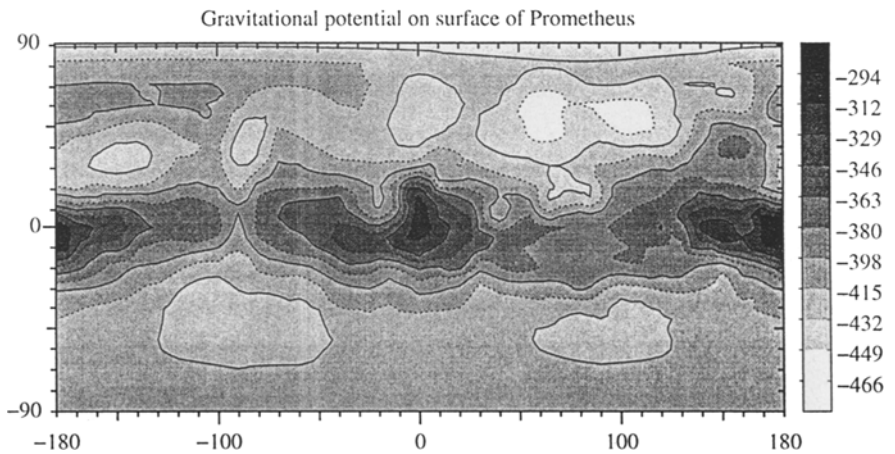

Fig. 20. The gravitational potential on the surface of Prometheus ($\mathrm{m}^2/\mathrm{s}^2$).

a constant g_r, we still do not account for the true *distance* between the measured and referenced point; this is because a direction to the referenced point could not be well defined, if the point is chosen on the equipotential surface (defined by the reference potential W_0).

Acknowledgements

We thank Prof. P. J. Stooke who supplied the data we used. This work was supported by KBN Research Grant No. 2 2104 92 03 and NCU Research Grant 386-A. We thank Prof. A. Drożyner for the possibility of usage SUN10/30 system for calculations (KBN Research Grant No. 2 2150 92 03p/14). We are thankful to

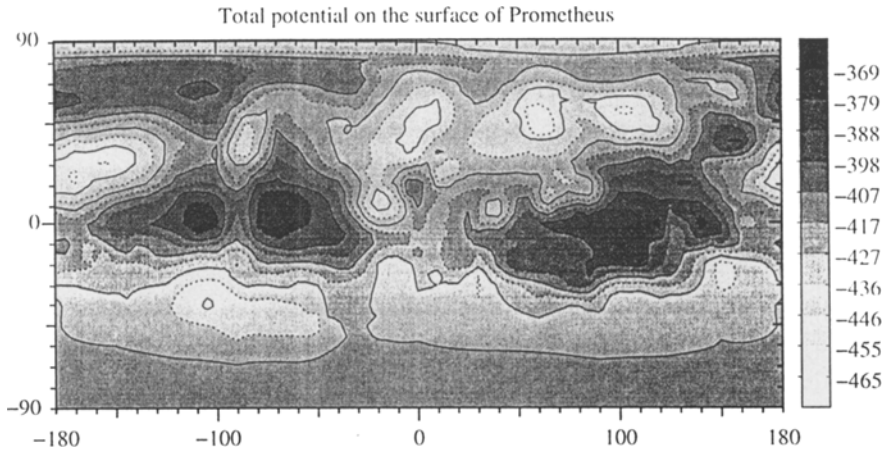

Fig. 21. The total potential (including self-gravity, rotation and tidal influence of Saturn) on the surface of Prometheus (m^2/s^2).

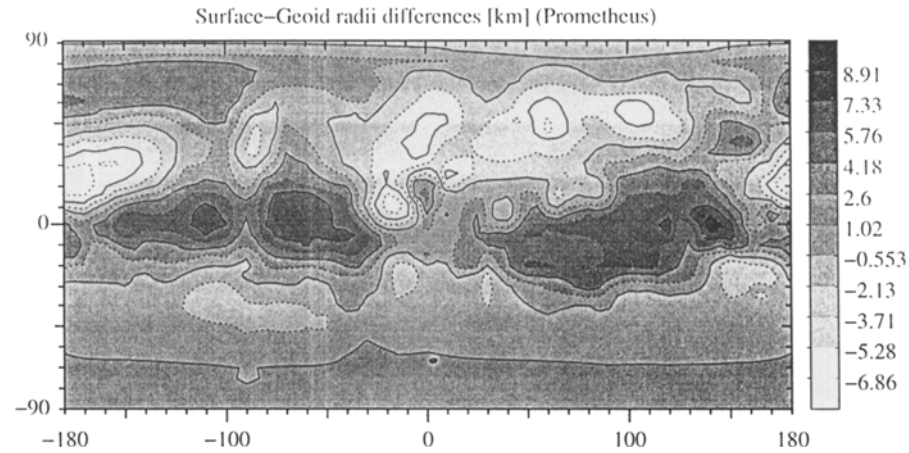

Fig. 22. Radial separation of the surface of Prometheus from the equipotential surface $W_0 = -419$ m^2/s^2.

Zbroja for her linguistic help. We wish to acknowledge Kenny Toh, who is the author of graphic package Plotmtv v.1.4, which was used for plotting contour maps.

Appendix

This appendix summarizes the formulae applied in this work. They come from the papers of (Martinec *et al.*, 1989) and (Goździewski *et al.*, 1994). Because of some misprints in the second paper, we decided to write a complete set of formulae.

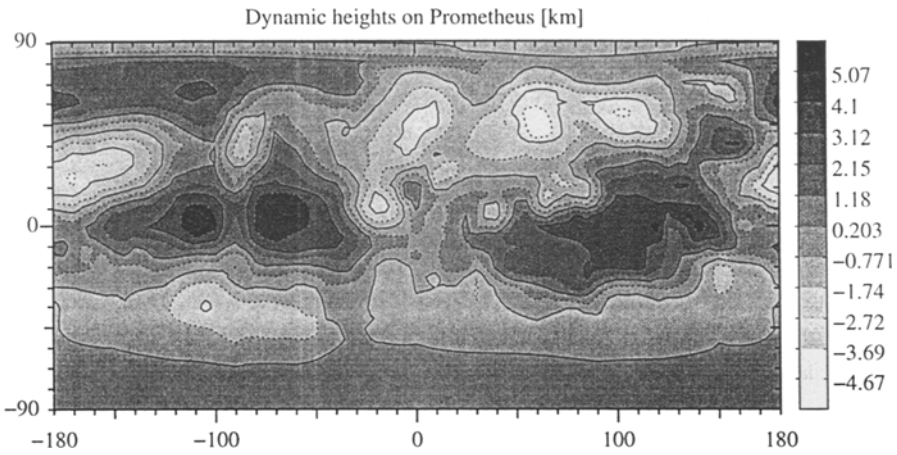

Fig. 23. Dynamic heights on Prometheus (km).

A. HARMONIC EXPANSION OF TOPOGRAPHY

We assume that coordinates of points are given in the body-fixed, planetocentric reference frame.

The radius of topography as the expansion in terms of the real spherical harmonics (Bills and Ferrari, 1978) is:

$$r_t(\phi,\lambda) = \sum_{j=0}^{j_{\max}} \sum_{m=0}^{m=j} \bar{P}_{jm}(\sin\phi)[\bar{a}_{jm}\cos(m\lambda) + \bar{b}_{jm}\sin(m\lambda)], \tag{A.1}$$

where (r_t, ϕ, λ) are spherical coordinates of a point of the body's surface. The set of coefficients $(\bar{a}_{jm}, \bar{b}_{jm})$ describes the shape completely.

The functions $\bar{P}_{jm}$ are normalized associated Legendre functions, i.e.,

$$\bar{P}_{jm}(x) = N_{jm} P_j^m(x), \quad N_{jm} = \sqrt{(2-\delta_{m0})(2j+1)\frac{(j-m)!}{(j+m)!}},$$

where

$$P_j^m(x) = \frac{(1-x^2)^{m/2}}{2^j j!}\frac{d^{j+m}(x^2-1)^j}{dx^{j+m}},$$

are unnormalized associated Legendre functions of degree j and order m.

The complex form of the topography expansion (Martinec *et al.*, 1989) is defined by:

$$r_t(\phi,\lambda) = \sum_{j=0}^{\infty} \sum_{m=j}^{m=-j} E_{jm} Y_{jm}(\phi,\lambda). \tag{A.2}$$

Now E_{jm} denote complex harmonic coefficients, and $Y_{jm}(\phi, \lambda) = P_{jm}(\sin\phi)e^{im\lambda}$ are fully normalized complex spherical harmonics.

The functions $P_{jm}(\sin\phi)$ are fully normalized associated Legendre functions. Their normalization is the same as the one widely used in quantum mechanics.

Relations between different forms of the Legendre functions are as follows:

$$P_{jm}(x) = (-1)^m \sqrt{\frac{(2j+1)(j-m)!}{4\pi(j+m)!}} P_j^m(x) \tag{A.3}$$

$$= (-1)^m \sqrt{\frac{1}{4\pi(2-\delta_{m0})}} \bar{P}_{jm}(x). \tag{A.4}$$

The complex, fully normalized harmonic coefficients E_{jm} have the form:

$$E_{jm} = (-1)^m \sqrt{\frac{4\pi(j+m)!}{(2j+1)(j-m)!}} \frac{1}{(2-\delta_{m0})} (a_{jm} - ib_{jm}) \tag{A.5}$$

$$= (-1)^m \sqrt{\frac{4\pi}{(2-\delta_{m0})}} (\bar{a}_{jm} - i\bar{b}_{jm}), \quad m \geq 0. \tag{A.6}$$

Here $\{a_{jm}, b_{jm}\}$ and $\{\bar{a}_{jm}, \bar{b}_{jm}\}$ denote real unnormalized and real fully normalized spectral harmonic coefficients, respectively. Because r_t is real, it follows that for $m \leq 0$ we have the following relations:

$$Y_{j,-m} = (-1)^m Y_{jm}^*, \qquad E_{j,-m} = (-1)^m E_{jm}^*,$$

where the symbol $*$ denotes the complex conjugation.

Natural k-th power of the radius of topography can be written as

$$\begin{aligned} r_t^k &= \sum_{j_1,m_1} \sum_{j_2,m_2} E_{j_1,m_1}^{(k-1)} E_{j_2,m_2}^{(1)} Y_{j_1,m_1} Y_{j_2,m_2} \\ &\equiv \sum_j \sum_m E_{jm}^{(k)} Y_{jm}, \qquad k > 1, \end{aligned} \tag{A.7}$$

where $E_{jm}^{(k-1)}$ are expansion coefficients of the $(k-1)$ power of r_t, $E_{jm}^{(1)} \equiv E_{jm}$. The general form of the coefficient is:

$$E_{jm}^{(k)} = \sum_{j_1,m_1} \sum_{j_2,m_2} \sqrt{\frac{(2j_1+1)(2j_2+1)}{4\pi(2j+1)}} C_{j_1 0 j_2 0}^{j0} C_{j_1 m_1 j_2 m_2}^{jm} E_{j_1,m_1}^{(k-1)} E_{j_2,m_2}^{(1)}, \tag{A.8}$$

where C and Clebsh–Gordan coefficients.

B. Geometric characteristics

The mean radius r_0 of the topography is defined as $r_0 \equiv \bar{a}_{00}$.

The mean equatorial radius is determined as (Martinec *et al.*, 1989)

$$a_e = \frac{1}{2\pi} \int_0^{2\pi} r_t(0, \lambda)\, \mathrm{d}\lambda,$$

and in terms of the topography expansion it is expressed by:

$$a_e = r_0 \left[1 + \sum_{j=1}^{\infty} (-1)^j \sqrt{\frac{4j+1}{4\pi}} \frac{(2j-1)!!}{(2j)!!} \right].$$

The mass M and volume V of a body having constant density $\rho(\mathbf{r}) = \rho_c$, are defined by

$$M = \rho_c \frac{2}{3} \sqrt{\pi} E_{00}^{(3)} \equiv \rho_c V, \quad \text{thus} \quad V = \frac{2}{3} \sqrt{\pi} E_{00}^{(3)}. \tag{B.1}$$

Offsets of the center of the body from the origin of the coordinates system are expressed by the formulae:

$$\bar{x} = -\frac{1}{2} \sqrt{\frac{3}{2}} \frac{\Re E_{11}^{(4)}}{E_{00}^{(3)}}, \quad \bar{y} = \frac{1}{2} \sqrt{\frac{3}{2}} \frac{\Im E_{11}^{(4)}}{E_{00}^{(3)}}, \quad \bar{z} = \frac{\sqrt{3}}{4} \frac{E_{10}^{(4)}}{E_{00}^{(3)}}. \tag{B.2}$$

C. Tensor of inertia

The inertia tensor (per mass unit) in terms of harmonic expansion of topography is detrmined by the following equations:

$$\begin{aligned}
I_{xx}/M &= \frac{2}{5} \left(E_{00}^{(5)} + \frac{1}{2\sqrt{5}} E_{20}^{(5)} - \sqrt{\frac{3}{10}} \Re E_{22}^{(5)} \right) \Big/ E_{00}^{(3)} \\
I_{yy}/M &= \frac{2}{5} \left(E_{00}^{(5)} + \frac{1}{2\sqrt{5}} E_{20}^{(5)} + \sqrt{\frac{3}{10}} \Re E_{22}^{(5)} \right) \Big/ E_{00}^{(3)} \\
I_{zz}/M &= \frac{2}{5} \left(E_{00}^{(5)} - \frac{1}{\sqrt{5}} E_{20}^{(5)} \right) \Big/ E_{00}^{(3)} \\
I_{xy}/M &= \frac{2}{5} \sqrt{\frac{3}{10}} \Im E_{22}^{(5)} / E_{00}^{(3)}, \\
I_{xz}/M &= \frac{2}{5} \sqrt{\frac{3}{10}} \Re E_{21}^{(5)} / E_{00}^{(3)}, \\
I_{yz}/M &= -\frac{2}{5} \sqrt{\frac{3}{10}} \Im E_{21}^{(5)} / E_{00}^{(3)}.
\end{aligned} \tag{C.1}$$

D. STOKES COEFFICIENTS

Denoting by G the gravitational constant, by M the mass of a body, by r_0 a reference radius, the external gravitational potential of the body at a point (ρ, ϕ, λ) can be written in the complex form (Martinec *et al.*, 1989) as:

$$U(\rho, \phi, \lambda) = \frac{GM}{r} \sum_{j=0}^{\infty} \left(\frac{r_0}{r}\right)^j \sum_{m=-j}^{m=j} A_{jm} Y_{jm}(\phi, \lambda), \tag{D.1}$$

where the coefficients of expansion are complex and fully normalized in the complex sense:

$$A_{jm} = \frac{6\sqrt{\pi}}{(j+3)(2j+1)} \frac{1}{r_0^j} \frac{E_{jm}^{(j+3)}}{E_{00}^{(3)}}. \tag{D.2}$$

Relation between the coefficients and their unnormalized and real representations is the same as in the case of topographic coefficients.

References

Antonov, V. A., Holshevnikov, K. V.: 1980, 'On the Possibility of the Use of Laplace Series for the Gravitational Potential on the Planet Surface', *Astron. Zh.* **57**(6), 1323–1330.

Bills, B. G. and Ferrari, A. J.: 1978, 'Mars Topography Harmonics and Geophysical Implications', *J. Geoph. Res.* **83**(B7), 3497–3508.

Chujkowa, N. A.: 1978, 'On the Use of Satellites Model of Potential on a Planet's Physical Surface', *Astron. Zh.* **55**(4), 862–872.

Chujkowa, N. A.: 1984, 'A New Proof of the Convergence of Laplace Series on Planet's Surfaces', *Vest. Moscow Univ.* **25**(1), 22–28.

Danby, J. M. A.: 1962, *Fundamentals of Celestial Mechanics*, The Macmillan Company, New York, pp. 98–107.

Fitzpatrick, P. M.: 1970, *Principles of Celestial Mechanics*, Academic Press, pp. 289–290.

Goździewski, K., Maciejewski, A. J., and Stooke, P. J.: 1994, 'A Model of the Gravitational Field of Amalthea. Part I: Derivation', *Earth, Moon and Planets* **64**, 243–264.

Kutshik, E. K.: 1990, 'On the Gravitational Field of Phobos', *Astron. Vest* **24**, 96–102.

Lang, K. R.: 1991, *Astrophysical Data: Planets and Stars*, Springer-Verlag, p. 74.

Martinec, Z., Pěč, K., and Burša, M.: 1989, 'The Phobos Gravitational Field Modeled on the Basis of its Topography', *Earth, Moon and Planets* **45**, 219–235.

Petrovskaya, M.S.: 1979, 'Estimation of Errors of the Satellite Model of the Potential on a Planetary Surface', *Astron. Zh.* **65**(1), 138–149.

Press, W. H., Tenkolsky, S. A., Vetterling, W. T., Flannery, B. P.: 1992, *Numerical Recipes in FORTRAN, The Art of Scientific Computing, Second Edition*, Cambridge Univ. Press.

Stooke, P. J.: 1994, 'The Shapes and Surface Features of Prometheus and Pandora', *Earth, Moon and Planets*, (in press).

Thomas, P. C.: 1994, 'Gravity, Tides, and Topography on Small Satellites and Asteroids: Application to Surface Features on the Martian Satellites', *Icarus*, in press.

Werner, R. A.: 1994, 'The Gravitational Potential of a Homogeneous Polyhedron or Don't Cut Corners', *Celest Mech.* **59**, pp. 253–278.

Veverka, J., Thomas, P., Davies, M., and Morrison, D.: 1981, 'Amalthea: Voyager Imaging Results', *J. Geoph. Res.* **86**(A10), 8675–8692.

Yoder, C. F., Synnott, S. P., and Salo, H.: 1989, 'Orbits and Masses of Saturn's Co-orbiting Satellites, Janus and Epimetheus', *Astron. J.* **98**(5), 1875–1889.